ACS OMEGA

Article

Narrow-Band SrMgAl$_{10}$O$_{17}$:Eu^{2+}, Mn^{2+} Green Phosphors for Wide-Color-Gamut Backlight for LCD Displays

Heejoon Kang, Keyong Nam Lee, Sanjith Unithrattil, Ha Jun Kim, Ji Hye Oh, Jae Soo Yoo, Won Bin Im,* and Young Rag Do*

Read Online

ACCESS | Metrics & More | Article Recommendations | Supporting Information

ABSTRACT: The strength of the photoluminescence excitation (PLE) spectrum of SrMgAl$_{10}$O$_{17}$:Eu^{2+}, Mn^{2+} (SAM:Eu^{2+}, Mn^{2+}) phosphor increased at deep blue (∼430 nm) and red-shifted from violet to deep blue with increasing concentrations of both Eu^{2+} ions Mn^{2+} ions. Eu^{2+}−Mn^{2+} energy transfer between Eu^{2+} ions in Sr−O layer and Mn^{2+} ions at Al−O tetrahedral sites was maximized, and the photoluminescence (PL) intensity of the narrow-band Mn^{2+} emission was improved by optimizing the concentrations of Eu^{2+} and Mn^{2+} ions. The PL emission spectrum of the (Sr$_{0.6}$Eu$_{0.4}$)(Mg$_{0.4}$Mn$_{0.6}$)Al$_{10}$O$_{17}$ (SAM:Eu^{2+}, Mn^{2+}) phosphor peaks was optimized at 518 nm at a full width at half-maximum (FWHM) of 26 nm under light-emitting diode (LED) excitation at 432 nm LED. The color gamut area of a color-filtered RGB triangle of down-converted white LEDs (DC-WLEDs) incorporated with optimum SAM:Eu^{2+}, Mn^{2+} green and K$_2$SiF$_6$:Mn^{4+} (KSF:Mn^{4+}) red phosphors is enlarged by 114% relative to that of the NTSC standard system in the CIE 1931 color space. The luminous efficacy of our DC-WLED was measured and found to be ∼92 lm/W at 20 mA. Increased energy transfers between dual activators and red-shifted band-edge and enhanced intensity of PLE spectrum indicate the possibility of developing dual-activated narrow-band green phosphors for wide-color gamut in an LCD backlighting system.
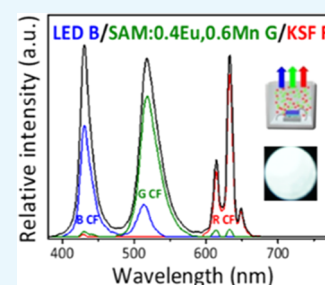
INTRODUCTION

Recently, quantum-dot-enhanced films (QDEFs) and QD powders have been commercialized to widen the color gamut of ultrahigh-definition (UHD) TVs, replacing rare-earth ion-doped inorganic phosphors.[1−5] Both CdSe/ZnS-based green (G) red (R) quantum-dot-enhanced film (QDEF)[4,5] and perovskite CsPbX$_3$ (X = Cl, Br, I)-based GR QD powders[13−16] guarantee a wider color gamut exceeding 120% of the NTSC standard in the 1931 Commission Internationale de l'Eclairage (CIE) x, y color space. However, both CdSe-containing QDs and perovskite QDs (PQDs) still have various disadvantages. First, they are all environmentally toxic and have short longevity, poor thermal stability, and mass production and cost issues.[7,8] Hence, nontoxic InP/ZnS QDs have been suggested as an alternative type of QD to replace CdSe-containing QDs and inorganic phosphors.[9,10] Although the best ever nontoxic InP/ZnS QDs yielded only approximately 100% of the NTSC standard, far below CdSe/ZnS QDs and PQDs,[11] nontoxic QDs have attracted much attention from backlight engineers as a viable alternative to rare-earth activated inorganic phosphors owing to the scarcity and cost of rare-earth elements as major components in most inorganic phosphors. However, the moderate bandwidth (∼35 nm) of G InP/ZnS QDs, as well as the reliability, photo-/thermostability, and longevity remain as critical issues with regard to the acceptance of nontoxic InP/ZnS QDs in the "on-chip" down-converted white light-emitting diode (DC-WLED) technology[11,12] (see Figure 1).

Given the drawbacks of each type of QDs, which prevent them from achieving a much wider color gamut for commercialized LCD backlight applications, it is necessary to develop narrow-band G and R inorganic phosphors.

Fortunately, the recent development of narrow-band Mn^{4+}-ion-doped fluoride and co-doped oxide R phosphors,[17−19] such as K$_2$SiF$_6$:Mn^{4+} (KSF:Mn^{4+}) and BaMgAl$_{10}$O$_{17}$:Mn^{4+}, Mg^{2+} (BAM:Mn^{4+}, Mg^{2+}) phosphors,[40] has provided a viable opportunity to develop a G phosphor to realize all-inorganic phosphor-based on-chip DC-WLED backlights as opposed to the use of "on-edge" or "on-film" (see Figure 1) type of QD-based backlight systems.[4,20] If it is possible to develop new types of environmentally viable and reliable G oxide phosphors with narrow full width at half-maximum values (FWHM < 30 nm) and a low synthetic cost, narrow-band G oxide phosphor will become a key component and will have a profound influence on the wide-color gamut of low-cost and highly reliable LCD backlighting applications. There are two approaches to develop a narrow-band G inorganic phosphor. As the first approach, similar to that of commercial β-SiAlON:Eu^{2+} G phosphor, many
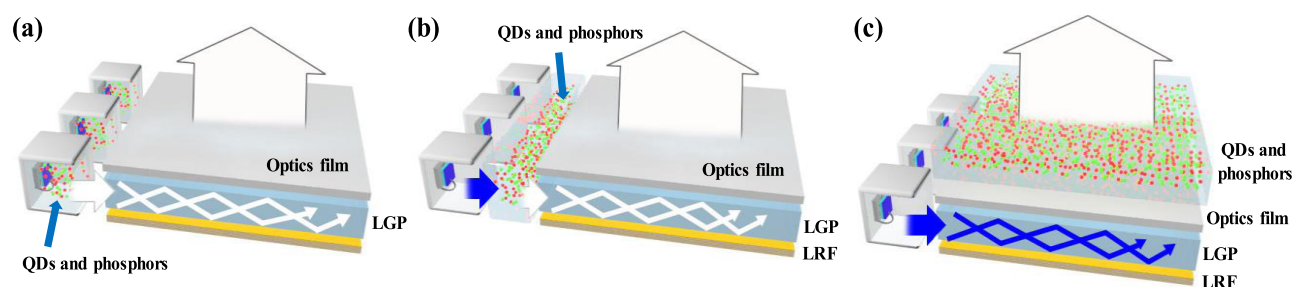
Figure 1. Three different structures of white-by-blue lighting systems in liquid crystal displays (LCDs) with the geometrical position of the QD or phosphors: (a) on-chip, (b) on-edge, and (c) on-film. QDs: quantum dots, LGP: light guide plate, LRF: light reflector film.

Table 1. Comparison of Optical Properties of White-by-Blue LEDs Containing Different Combinations of Inorganic Green and Red Phosphors

green phosphors	full width at half-maximum (nm)	emission pea (nm)	red phosphors	color Gamut (%) (with color filter)		luminous efficacy (lm/W)	correlated color temperature (K)		refs
				CIE 1931	CIE 1976				
β-sialon:Eu^{2+}	~55	535	$CaAlSiN_3$:Eu^{2+}	82.1	91.9	38		8620	NIMS [21]
$Sr_3Si_{12}Al_3O_2N_{21}$:Eu^{2+}	~65	520	$CaAlSiN_3$:Eu^{2+}	85.9	94.2	41		12 723	Toshiba[22]
$SrGa_2S_4$:Eu^{2+}	~50	530	K_2SiF_6:Mn^{4+}	86.4	N/A	105		8330	Kookmin U [23]
sharp β-sialon:Eu^{2+}	54	535	K_2SiF_6:Mn^{4+}	95.7	107.1			10 014	Sharp/ NIMS [6]
$Ba_2LiSi_7AlN_{12}$:Eu^{2+}	61	515							[27]
$Ba[Li_2(Al_2Si_2)N_6]$:Eu^{2+}	57	532							[28]
$RbLi(Li_3SiO_4)_2$:Eu^{2+}	42	530	K_2SiF_6:Mn^{4+}	107		97.28		6221	[44]
$RbNa(Li_3SiO_4)_2$:Eu^{2+}	41	523	K_2SiF_6:Mn^{4+}	113		111.08		5196	[45]
γ-AlON:Mn^{2+}, Mg^{2+}	44	520	K_2SiF_6:Mn^{4+}	102.4	110.8				[43]
$Sr_2MgAl_{22}O_{36}$:Mn^{2+}	26	518	K_2SiF_6:Mn^{4+}	127					[39]
$SrMgAl_{10}O_{17}$:Eu^{2+},Mn^{2+}	26	518	K_2SiF_6:Mn^{4+}	114	118	92		11 806	this work

recent studies have shown the development of novel narrow-band Eu^{2+}-doped nitride phosphors, such as $Ba_2LiSi_7AlN_{12}$:Eu^{2+} and $Ba[Li_2(Al_2Si_2)N_6]$:Eu^{2+} phosphors, as summarized in Table 1[6,21−26,39,43−45] However, Eu^{2+}-doped nitride G phosphors continue to be associated with broad-band emission and a high synthesis cost;[27−29] therefore, as a second approach, more attention has recently been paid to Mn^{2+}-activated G phosphors. These materials are much less expensive and may possess narrow-band emission features.[30−32] Recent studies have investigated Mn^{2+}-doped oxynitride and oxide phosphors such as sharp γ-AlON:Mn^{2+}, Mg^{2+} oxynitride and $BaMgAl_{10}O_{17}$:Mn^{2+} or $BaMgAl_{10}O_{17}$:Mn^{2+}, Eu^{2+} oxide for the development of narrow-band G phosphor candidates for application to DC-WLEDs. The FWHM of γ-AlON:Mn^{2+}, Mg^{2+} is still wider than 30 nm, an undesirable value, and Mn^{2+}-doped $BaMgAl_{10}O_{17}$ phosphors still have low external quantum efficiency (EQE) levels under blue excitation. Zhu et al. have recently developed another $Sr_2MgAl_{22}O_{36}$:Mn^{2+} (SMAO:Mn^{2+}) G phosphor using weak electric−phonon interaction caused by a highly rigid crystal structure, low structural disorder and relaxation due to highly symmetric tetrahedron, and single crystallographic sites around Mn^{2+} doping;[39] they found a new crystal structure that maintains a narrow-band photoluminescence (PL) emission spectrum. However, it is likely that Zhu's approach is not a simple means of finding new inorganic phosphors that meet the above-mentioned complex crystallographic requirements. Therefore, to increase the PL efficiency of the blue-excited G emission without significantly changing the crystallographic structure or narrow G emission, we also examined a dual-

activator-co-doped $SrMgAl_{10}O_{17}$:Eu^{2+}, Mn^{2+} phosphor. Fortunately, the stability of structures of $MMgAl_{10}O_{17}$-based (M = Ba, Sr, or Ca) phosphors is well known because $BaMgAl_{10}O_{17}$:Eu^{2+} phosphors have been commercially utilized as blue phosphors for fluorescent lamp (FL) and plasma display panel (PDP) applications.[41,42] To increase the PL efficiency of the narrow-band G emission of Mn^{2+} activators, we attempted to optimize the energy transfer between Eu^{2+}−Mn^{2+} ions and thereby increase the intensity and red shift of the photoluminescence excitation (PLE) band edge at deep blue wavelength (~430 nm). This was achieved by uniform doping of highly concentrated dopants and by utilizing the structural miscibility of similar ion sizes between octacoordinated Sr^{2+} (1.26 Å) and Eu^{2+} (1.25 Å).[46] First, we analyzed and optimized the concentration effect of Eu^{2+} ions on the energy transfer between Eu^{2+}−Mn^{2+} ions of $(Sr_{1−x}Eu_x)(Mg_{0.4}Mn_{0.6})Al_{10}O_{17}$ G phosphors as a G component in white-by-blue LED applications. In relation to this, we synthesized and characterized a series of $(Sr_{1−x}Eu_x)(Mg_{0.4}Mn_{0.6})Al_{10}O_{17}$ (x = 0.01, 0.05, 0.1, 0.2, 0.4, 0.6, 0.8, 1.0) phosphors using a solid-state reaction. Second, we studied the effects of concentration of Mn^{2+} ions on the intensity of the PLE spectrum, the red shift of the PLE band edge, and the PL efficiency of $(Sr_{0.6}Eu_{0.4})(Mg_{1−y}Mn_y)Al_{10}O_{17}$ G phosphors as a function of Mn^{2+} ions in Mg^{2+} sites in orderly layered structure crystals of $SrMgAl_{10}O_{17}$ (SAM). As part of this effort, we synthesized and characterized $(Sr_{0.6}Eu_{0.4})(Mg_{1−y}Mn_y)Al_{10}O_{17}$ (y = 0.1 ~ 0.9) G phosphors. These systematic optimization approaches confirmed that an optimum $(Sr_{0.6}Eu_{0.4})$-$(Mg_{0.4}Mn_{0.6})Al_{10}O_{17}$ (SAM:$0.4Eu^{2+}$, $0.6Mn^{2+}$) phosphor results

in a narrow-band G phosphor for use in a white-by-deep-blue backlight system. We used an on-chip type of WLED in an LCD backlight system to test possible G phosphor candidates as LCD backlights. The color gamut of the filtered narrow-band G-emitting SAM:0.4Eu^{2+},0.6Mn^{2+} and R-emitting KSF:Mn^{4+}-based white-by-blue (114%) is wider than those of the sharp γ-AlON:Mn^{2+}, Mg^{2+} G and KSF:Mn^{4+} R phosphor-based tricolor WLEDs ($\sim$102%)[6] and slightly narrower than that of the SMAO:Mn^{2+} G and KSF:Mn^{4+} R phosphor-based tricolor WLEDs (127%).[39] However, the resultant color gamut of the filtered dual-activator SAM-based WLED is still superior to the widest color gamut ($\sim$100%) of commercialized InP/ZnS QDEF WLEDs reported thus far. This approach of increased energy transfer between dual activators and a red-shifted band-edge of the PLE spectrum suggests the suitability of developing novel narrow-band G phosphors as a platform material with narrow-band emission spectrum for a wide-color-gamut LCD backlighting system because BAM family (MMgAl$_{10}$O$_{17}$:Mn^{2+}, Eu^{2+}, M = Ba^{2+}, Sr^{2+}, Ca^{2+}, and Eu^{2+}) phosphors have a stable crystal structure and because these phosphors are already commercialized.

■ RESULTS AND DISCUSSION

SAM crystallizes as an orthorhombic structure with space group $P6_3/mmc$ and has a β-Al$_2$O$_3$-type layered structure (β-alumina structure). As has been well established, MgAl$_{10}$O$_{16}$ spinel blocks are sandwiched between or separated by Sr-O conduction layers (or mirror planes).[33−35] It was also reported that Eu^{2+} ions can partially replace Sr^{2+} ion sites in the conduction layer and that Mn^{2+} can replace Mg^{2+} ions in the spinel blocks, as shown in Figure 2[32] As reported by Yamamoto
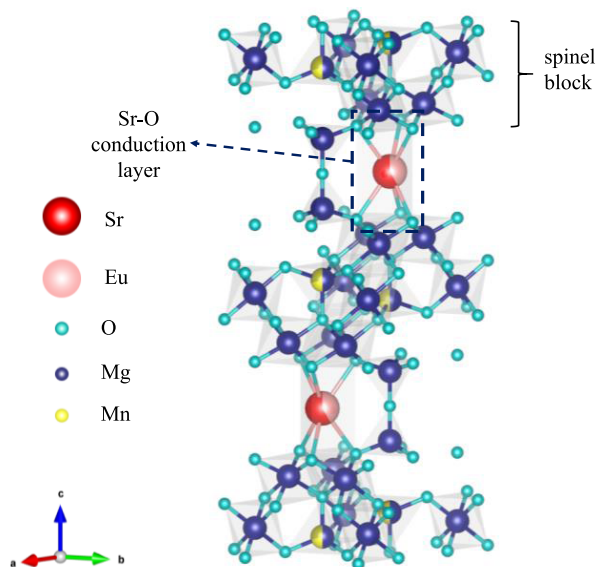

Figure 2. β-Alumina structure of the SrMgAl$_{10}$O$_{17}$:Eu,Mn phosphor: the Eu^{2+} ion replaces the Sr^{2+} ion in the Sr−O conduction layer, and the Mn^{2+} ion replaces the Mg^{2+} ion in the MgAl$_{10}$O$_{16}$ spinel blocks.

et al., a high concentration of Mn^{2+} dopants in BAM hosts can induce high absorption efficiency for near-UV excitation and consequently result in high G PL output under UV excitation without a concentration quenching process.[31] In a close match with the PLE spectrum of the BAM:0.45Mn^{2+} G phosphor in a previous report, one broad peak and three sharp peaks were found at 340 nm and at 255, 428, and 455 nm, respectively,

which were assigned to 3d−3d electronic transitions (see ref 31). As a result, the PL of BAM:0.45Mn^{2+} shows an efficient G spectrum centered at 518 nm, and the FWHM of the PL emission spectrum is approximately 25 nm. As expected, the CIE chromaticity coordinates of BAM:Mn^{2+} are located at the purer G color of x = 0.147 and y = 0.744. In this study, instead of studying BAM:Eu^{2+}, Mn^{2+} phosphors, we examined SAM:Eu^{2+}, Mn^{2+} phosphors because the similar sizes between Sr^{2+} (1.26 Å) and Eu^{2+} (1.25 Å) ions provide a benefit of homogeneous distribution of dopant ions even at a high concentration of Eu^{2+} ions, which assists with energy transfer between Eu^{2+} and Mn^{2+} ions in a hexagonal structure. Therefore, by replacing Sr^{2+} with Eu^{2+} in SAM:Eu^{2+}, Mn^{2+} phosphors, we can increase energy transfer and extend the right-hand side of the PLE spectrum at half the maximum of the envelope by 15−20 nm, toward the red region of the spectra with a wavelength as high as 428 nm. As shown in Figure 3, the excitation spectrum of Eu^{2+}- and Mn^{2+}-
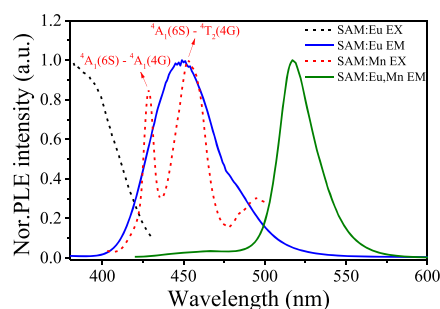

Figure 3. Excitation spectrum of SAM:Eu, SAM:Mn and emission spectrum of SAM:Eu and Eu^{2+}- and Mn^{2+}-co-doped SAM:Eu,Mn.

co-doped SAM shows a broad band corresponding to the 4f−5d transition of the Eu^{2+} ions, while also showing two sharp peaks at 427 and 455 nm, corresponding to the transitions from $^4A_1(6S)$ to $^4A_1(4G)$ and $^4A_1(6S)$ to $^4T_2(4G)$ of the Mn^{2+} ions.[31] It was reported that the spectral overlap between the emission of SAM:Eu^{2+} and the excitation of SAM:Mn^{2+} in the blue wavelength range induces an effective energy transfer from Eu^{2+} to Mn^{2+} in the Eu^{2+}- and Mn^{2+}-co-doped SAM phosphor.[35] As is well known, the replacement of similar-sized Eu^{2+} cations keeps the lattice parameters of the crystal structure nearly the same, as shown in Figure S2, and the high concentration of Eu^{2+} ions can decrease the distance between the Eu^{2+} ions and Mn^{2+} ions, thereby increasing the possibility of energy transfer between the Eu^{2+} ions and Mn^{2+} ions.[36]

As shown in Figure 4a,b, X-ray diffraction (XRD) patterns of both the (Sr$_{1−x}$Eu$_x$)(Mg$_{0.4}$Mn$_{0.6}$)Al$_{10}$O$_{17}$ (x = 0.0, 0.01, 0.05, 0.1, 0.2, 0.4, 0.6, 0.8, 1.0) and (Sr$_{0.6}$Eu$_{0.4}$)(Mg$_{1−y}$Mn$_y$)Al$_{10}$O$_{17}$ (y = 0.1, 0.2, 0.3, 0.4, 0.5, 0.6, 0.7, 0.8, 0.9) G phosphor series match those of the pure hexagonal phase (JCPDS card no. 00-026-0879). As previously reported, this SAM phase consists of two SrAl$_{10}$O$_{16}$ spinel blocks and one Sr−O conduction layer. Therefore, it was reported that Eu^{2+} replaces Sr^{2+} ions in the Sr−O conduction layer and that Mn^{2+} replaces Mg^{2+} ions in the SrAl$_{10}$O$_{16}$ spinel block, without significantly changing the crystal structure.

Figure 4a shows that, owing to the similar ionic radius of Eu^{2+} (1.25 Å) compared to that of Sr^{2+} (1.26 Å),[37] the spacing between the two peaks of the (008) and (107) planes remains almost identical within the experimental error range with an increase in the amount of substituted Eu^{2+} from x = 0.4 to 1.0 in the (Sr$_{1−x}$Eu$_x$)(Mg$_{0.4}$Mn$_{0.6}$)Al$_{10}$O$_{17}$ system. The similar relation-
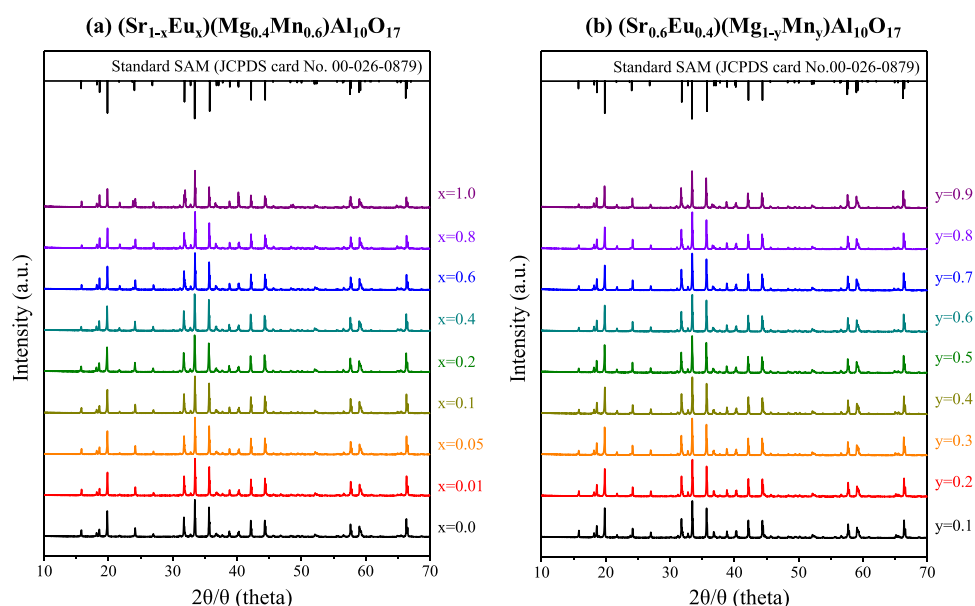
Figure 4. XRD patterns of (a) $(Sr_{1-x}Eu_x)(Mg_{0.4}Mn_{0.6})Al_{10}O_{17}$ ($x = 0.0, 0.01, 0.05, 0.1, 0.2, 0.4, 1.0$) and (b) $(Sr_{0.6}Eu_{0.4})(Mg_{1-y}Mn_y)Al_{10}O_{17}$ ($y = 0.0, 0.1, 0.2, 0.3, 0.4, 0.5, 0.6, 0.7$).

Table 2. Rietveld Refinement and Crystal Parameter Data of $(Sr_{1-x}Eu_x)(Mg_{0.4}Mn_{0.6})Al_{10}O_{17}$[a]N

formula	$(Sr_{1-x}Eu_x)(Mg_{0.4}Mn_{0.6})Al_{10}O_{17}$					
	$x = 0.0$	$x = 0.2$	$x = 0.4$	$x = 0.6$	$x = 0.8$	$x = 1.0$
radiation type			synchrotron			
2θ range (degree)			10−130			
T (K)			295			
symmetry			hexagonal			
space group			$P63/mmc$			
Z			2			
$a = b$ (Å)	5.630183(5)	5.630242(7)	5.631227(5)	5.631714(6)	5.631887(6)	5.632014(7)
c (Å)	22.404100(34)	22.407396(46)	22.408907(32)	22.408321(37)	22.410187(40)	22.414896(47)
V (Å³)	615.041(1)	615.099(1)	615.400(1)	615.490(1)	615.503(1)	615.736(1)

[a]Numbers within parentheses are the estimated standard deviations of the last significant figure.

Table 3. Rietveld Refinement and Crystal Parameter Data of $(Sr_{0.6}Eu_{0.4})(Mg_{1-y}Mn_y)Al_{10}O_{17}$[a]

formula	$(Sr_{0.6}Eu_{0.4})(Mg_{1-y}Mn_y)Al_{10}O_{17}$				
	$y = 0.1$	$y = 0.2$	$y = 0.4$	$y = 0.6$	$y = 0.8$
radiation type			synchrotron		
2θ range (degree)			10−130		
T (K)			295		
symmetry			hexagonal		
space group			$P63/mmc$		
Z			2		
$a = b$ (Å)	5.625397(7)	5.626466(6)	5.628942(9)	5.631227(5)	5.633628(9)
c (Å)	22.391886(49)	22.395170(40)	22.409492(60)	22.408907(32)	22.421360(68)
V (Å³)	613.660(1)	613.983(1)	614.914(2)	615.400(1)	616.232(1)

[a]Number within parentheses are the estimated standard deviations of the last significant figure.

ship between the XRD peak position and the composition indicates that $SrMgAl_{10}O_{17}$ forms a perfectly solid solution with $EuMgAl_{10}O_{17}$. The detailed structural information and the influence of ionic substitution on $(Sr_{0.6}Eu_{0.4})(Mg_{0.4}Mn_{0.6})$-$Al_{10}O_{17}$ were analyzed through Rietveld refinement, as shown in Figure S1. The refinement converged such that the R_{wp} value and goodness-of-fit parameter (χ^2) were in acceptable ranges; structural parameters of $(Sr_{0.6}Eu_{0.4})(Mg_{0.4}Mn_{0.6})Al_{10}O_{17}$ are shown in Tables S2 and S3. The obtained refinement parameters

and the unit cell parameters of both the $(Sr_{1-x}Eu_x)(Mg_{0.4}Mn_{0.6})$-$Al_{10}O_{17}$ and $(Sr_{0.6}Eu_{0.4})(Mg_{1-y}Mn_y)Al_{10}O_{17}$ series are tabulated in Tables 2 and 3, respectively. Most of the compounds were found to be of single-phase type, while a few of them showed the nominal presence of impurity phases. The evolution outcomes of the lattice parameter of the compound series for similar values of x and y are shown in Figures S2 and S3, respectively. The introduction of a similar size of Eu^{2+} in place of Sr^{2+} resulted in a negligible lattice change along the c axis, as well as along the a/b

axis. Furthermore, the introduction of Mn^{2+} resulted in a slight increase of the lattice parameter along both the a/b and c axes due to an increase of ionic radius, as shown in Figure S3 (4-coordinated, Mg^{2+} = 0.57 Å, Mn^{2+} = 0.66 Å). Therefore, the negligible effect of volume change by Mn^{2+} replacement in $MgAl_{10}O_{16}$ spinel blocks and by Eu^{2+} replacement in the Sr−O conduction layer confirmed the uniform doping of Eu^{2+} ions even when there were high concentrations of both Eu^{2+} and Mn^{2+} ion in the doped SAM:Eu^{2+}, Mn^{2+} phosphor.

Figure 5a−c shows relative PLE, normalized PLE, and relative PL spectra of the $(Sr_{1−x}Eu_x)(Mg_{0.4}Mn_{0.6})Al_{10}O_{17}$ G phosphor
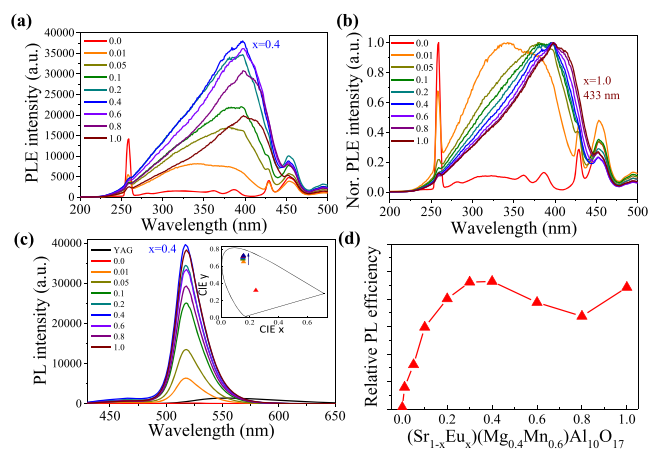
Figure 5. (a) Relative PLE spectra at λ_{em} = 518 nm and (b) normalized PLE spectra of $(Sr_{1−x}Eu_x)(Mg_{0.4}Mn_{0.6})Al_{10}O_{17}$ (x = 0.01, 0.05, 0.1, 0.2, 0.4, 0.6, 0.8, 1.0) phosphors at λ_{ex} = 400 nm. (c) Relative PL spectra at λ_{em} = 518 nm and CIE color coordinates of $(Sr_{1−x}Eu_x)(Mg_{0.4}Mn_{0.6})Al_{10}O_{17}$ phosphors at λ_{ex} = 400 nm (inset) and (d) PL efficiency vs Eu concentration of $(Sr_{1−x}Eu_x)(Mg_{0.4}Mn_{0.6})Al_{10}O_{17}$ phosphors at λ_{ex} = 400 nm.

series. The PLE spectra of Eu^{2+} in both sample series show a broad-band feature, which corresponds to the 4f−5d transition of Eu^{2+} ions, implying that this Eu^{2+}- and Mn^{2+}-co-doped phosphor can be efficiently excited by near-UV light and deep blue light. The increased intensity of the deep blue PLE spectrum with the increase in the concentration of Eu^{2+} ions indicates increased energy transfer between Eu^{2+} ions located in the Sr^{2+} sites and Mn^{2+} ions located in the Mg^{2+} sites, which in turn decreases the distance between the Eu^{2+} and ions Mn^{2+}, resulting in an increase of the 3d−3d transition. Therefore, the intensity of PLE at 432 nm and the right-hand side of PLE at the half-maximum shifts from ∼411 to ∼433 nm (see Figure 5b), indicating that the highly concentrated Eu^{2+} ions (x > 0.2) of the $(Sr_{1−x}Eu_x)(Mg_{0.4}Mn_{0.6})Al_{10}O_{17}$ phosphor are excitable by deep B LED sources (∼430 nm), as well as by near-UV light.

Upon excitation at 400 nm, the PL spectra of both $(Sr_{1−x}Eu_x)(Mg_{0.4}Mn_{0.6})Al_{10}O_{17}$ samples consist of B and G emission bands. The B and G emissions here apparently correspond to the 4f−5d and 3d−3d transitions from Eu^{2+} and Mn^{2+} ions. With the energy transfer between the two activators, the relative intensities of the B emissions are reduced and finally mostly disappear due to the increasing concentration of Mn^{2+} ions (Figure 6c). As previously reported, an efficient energy transfer occurs between the emitted energy of Eu^{2+} and the absorbed energy of Mn^{2+} ions because of the shorter distance (5.9−6.2 Å) between Eu^{2+} and Mn^{2+} compared to the critical distance (10.9 Å) of energy transfer of co-doped BAM phosphors. This energy transfer was mainly of resonance type
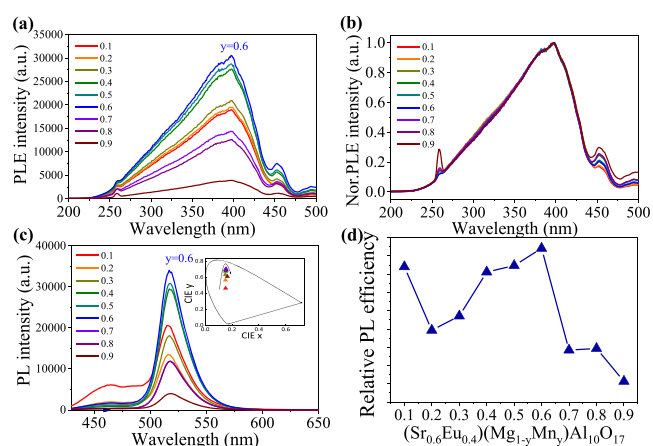

Figure 6. (a) Relative PLE spectra at λ_{em} = 518 nm and (b) normalized PLE of $(Sr_{0.6}Eu_{0.4})(Mg_{1−y}Mn_y)Al_{10}O_{17}$ (y = 0.1, 0.2, 0.3, 0.4, 0.5, 0.6, 0.7, 0.8, 0.9) phosphors at λ_{ex} = 400 nm. (c) Relative PL spectra at λ_{em} = 518 nm and CIE color coordinates of $(Sr_{0.6}Eu_{0.4})(Mg_{1−y}Mn_y)Al_{10}O_{17}$ phosphors at λ_{ex} = 400 nm (inset). (d) PL efficiency vs Mn concentration of $(Sr_{0.6}Eu_{0.4})(Mg_{1−y}Mn_y)Al_{10}O_{17}$ phosphors at λ_{ex} = 400 nm.

via electric dipole−quadrupole interaction.[38] As a result of energy transfer, most of the pure G emission is obtained from the concentration of Eu^{2+} above 0.2 when the Mn^{2+} concentration is 0.6. Similar to the change in the PL spectrum, the CIE color coordinates of the $(Sr_{1−x}Eu_x)(Mg_{0.4}Mn_{0.6})Al_{10}O_{17}$ phosphors moved from a bluish G color to a pure G color when the Eu^{2+} concentration exceeded x = 0.2 (Figure 5c, inset). As shown in Figure 5c, the maximum PLQY of the $(Sr_{1−x}Eu_x)-(Mg_{0.4}Mn_{0.6})Al_{10}O_{17}$ phosphors was also obtained from the optimum Eu concentration, x = 0.4. Therefore, the extension of the PLE spectrum to deep blue (∼430 nm) and the efficient transfer between Eu^{2+} and Mn^{2+} ions make the Eu^{2+}- and Mn^{2+}-co-doped SAM phosphor suitable for use as a G component in WLEDs using deep B LED chips.

To optimize the Mn concentration of the $(Sr_{0.6}Eu_{0.4})-(Mg_{1−y}Mn_y)Al_{10}O_{17}$ (y = 0.1−0.9) phosphor series, the optical properties (PLEs and PLs) of the G phosphors in this phosphor series are compared for increase in the concentration of Mn^{2+} ions (Figure 6a,b). The right-hand-side wavelengths of the PLE spectrum are located in a similar range, from 425 to 433 nm, due to the 3d−3d transition in Mn^{2+}, which is less affected by crystal field splitting. The blue PL peaks decreased slightly with increase in the concentration of Mn^{2+} ions. Maximum red shift and pure G color were obtained above a Mn^{2+} concentration of 0.3. The PL efficiency of the dual colors of the $(Sr_{0.6}Eu_{0.4})(Mg_{1−y}Mn_y)-Al_{10}O_{17}$ (y = 0.1−0.9) phosphor series increases to a Mn^{2+} concentration of 0.6 when the Eu^{2+} concentration is 0.4, as shown in Figure 6c. Although concentration quenching of the dual colors in the $(Sr_{0.6}Eu_{0.4})(Mg_{1−y}Mn_y)Al_{10}O_{17}$ G phosphor series occurs above a Mn^{2+} concentration of 0.6, consideration of the four parameters of the PL intensity of the G emission, the filtered G emission, the G purity of the PL peaks, and the band edge of PLE peaks indicates that the optimum concentrations of Eu^{2+} and Mn^{2+} ions can be obtained at high values of above x = 0.4 and y = 0.6, respectively (see Figure 6c). The highest PLQY of $(Sr_{0.6}Eu_{0.4})(Mg_{1−y}Mn_y)Al_{10}O_{17}$ (y = 0.1−0.9) phosphors was also obtained from the high concentration of Mn^{2+} ion, y = 0.6. Accordingly, the SAM:$0.4Eu^{2+}$, $0.6Mn^{2+}$ phosphor, as a suitable candidate Eu^{2+}- and Mn^{2+}-optimized phosphor, shows an efficient PL peak centered at 518 nm, and the FWHM of the

PL peak is close to ~26 nm (see Figure 6c), resulting in a strong narrow-band G spectrum with a small blue peak and a strong narrow-band pure G spectrum after filtration by a G filter. The CIE chromaticity coordinates of $(Sr_{0.6}Eu_{0.4})(Mg_{1-y}Mn_y)Al_{10}O_{17}$ ($y = 0.1-0.9$) phosphors move from bluish green to deep green with increase in the concentration of Mn^{2+} ions. The CIE chromaticity coordinates of the optimum green sample are located in the pure G color area in the CIE color diagram shown in Figure 6d. It is worth noting that the SAM structure has sandwiched layers alternating Sr—O and spinel blocks.

Thus, energy transfer between $Mn^{2+}-Mn^{2+}$ in spinel should be restricted to the Sr—O conduction layer and vice versa, which restriction can yield compounds that have a high critical value of concentration quenching along with structural flexibility. Therefore, the direct excitation band of Mn^{2+} in the deep B range can be increased dramatically, along with $Eu^{2+}-Mn^{2+}$ energy transfer. In order to find a proper G candidate for backlight application of DC-WLEDs, Table S1 compares and summarizes the relative PLQYs and other optical properties of the three different G phosphors (SAM:Mn^{2+}, dual-color SAM:Eu^{2+}, Mn^{2+} and pure G color SAM:Eu^{2+}, Mn^{2+}) under blue excitations of 418, 424, 432 and 447 nm. Here, the PL-efficient dual-color candidate and the purest G candidate are selected for the SAM:0.4Eu^{2+}, 0.6Mn^{2+} phosphor, which has a relatively high PLQY of ~0.98 at 430 nm excitation compared to YAG:Ce phosphor and absolute PLQY of ~0.28 at 430 nm excitation. The CIE chromaticity coordinates of the efficient SAM:0.4Eu^{2+}, 0.6Mn^{2+} G phosphor are $x = 0.148$ and $y = 0.757$ (Figure 7a, inset). The pure SAM:0.4Eu^{2+}, 0.6Mn^{2+} G phosphor
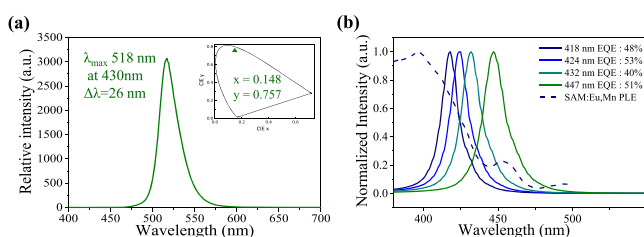

Figure 7. (a) PL spectrum of the SAM:0.4Eu,0.6Mn phosphor excited by 430 nm. The inset shows the CIE color coordinates of the SAM:0.4Eu, 0.6Mn phosphor. (b) Overlapping between the PLE spectrum of the SAM:0.4Eu, 0.6Mn phosphor at λ_{em} = 518 nm and a series of blue peaks and EQEs of various LEDs from 418 to 447 nm.

is one of the purest ever G color phosphors to be excitable by B LED chips, as shown in Figure 7a. Figure 7b shows the overlapped spectra of the PLE of the best SAM:0.4Eu^{2+}, 0.6Mn^{2+} phosphor and the EL spectra of various wavelength-tunable B LEDs. This figure indicates that the 432 nm blue LED is properly selected for use as an excitation source for a SAM:0.4Eu^{2+}, 0.6Mn^{2+} pure G phosphor and as a B source for one white LED incorporated with SAM:0.4Eu^{2+}, 0.6Mn^{2+} G color and KSF:Mn^{4+} R color phosphors.

In the last section, to verify the suitability of the SAM:0.4Eu^{2+}, 0.6Mn^{2+} pure G color phosphor in actual LED applications, white LEDs are fabricated by dispensing both SAM:Eu^{2+}, Mn^{2+} and KSF:Mn^{4+} mixed phosphor pastes onto a deep blue LED chip (~432 nm). Here, ~11 806 K white LEDs using SAM:Eu^{2+}, Mn^{2+} phosphors can be obtained by varying the SAM:Eu^{2+}, Mn^{2+} and KSF:Mn^{4+} R phosphor concentrations on a 432 nm B LED package. As previously reported, ~11 806 K white color is tuned by balancing the three colors of InGaN LED B-emitted

light, SAM:Eu^{2+}, Mn^{2+} G-emitted light, and KSF:Mn^{4+} R-emitted light.

To evaluate the suitability of SAM:Eu^{2+}, Mn^{2+} of the optimized pure G phosphors for further use in tricolor DC-WLEDs with a KSF:Mn^{4+} R phosphor for LCD backlighting applications, the white emission of a 11 806 K DC-WLED is spectrally resolved into its primary RGB colors by applying commercialized LCD RGB color filters. Figure 8a shows the transmittance spectra of the commercial B, G and R color filters. Individual colors of the full-color LCD displays are realized through the control of transmitted RGB light from LED backlights passing through the RGB color filters. Figure 8b provides the EL/PL spectra and color coordinates of a B LED, a KSF:Mn^{4+} R phosphor, and a SAM:Eu^{2+}, Mn^{2+} G phosphor. To measure the transmittance spectrum of white light passing through each RGB color filter, the RGB monochromatic spectrum and color gamut area are computed with white light from tricolor, single-package DC-WLEDs (Figure 8c). The insets in Figure 8d are actual photographs of white light and filtered RGB light from two tricolor WLEDs incorporating SAM:Eu^{2+}, Mn^{2+} G and KSF:Mn^{4+} R phosphors. Figure 8d,e displays the measured RGB spectra and CIE color coordinates from the filtered DC-WLEDs of a tricolor DC-WLED with SAM:Eu^{2+}, Mn^{2+} G and KSF:Mn^{4+} R phosphors. The R, G, and B emissions of the tricolor DC-WLED correspond to CIE color coordinates of (0.692, 0.300), (0.165, 0.742), and (0.155, 0.078), respectively, after filtration with color filters. The color gamut areas of the filtered RGB triangles of the two tricolor DC-WLEDs were calculated and found to be 114% relative to the NTSC standard system in the CIE 1931 color space. Therefore, the optimum SAM:Eu^{2+}, Mn^{2+} G phosphor for LCD backlight applications is determined here as an SAM:0.4Eu^{2+}, 0.6Mn^{2+} pure G color. The white emission of the 11806 K DC-WLED shows a good luminous efficacy (LE) (~92 lm/W at 20 mA). Figure 8f shows the LE value variations of a DC-WLED incorporated with SAM:0.4Eu^{2+}, 0.6Mn^{2+} G and KSF:Mn^{4+} R phosphors as a function of the applied current (mA) and operating temperature. Both the operating current and temperature stability of the SAM:Eu^{2+}, Mn^{2+} G phosphor show a degradation trend similar to that of the KSF:Mn^{4+} R phosphor, with acceptable changes of the CIE color coordinates, though the LE of the WLEDs decreases with an increase in the current density and operating temperature, similar to the trends reported in most phosphor applications studied in relation to WLEDs. The temperature and current stability of the SAM:Eu^{2+}, Mn^{2+} G phosphor indicate that the dual-activator-doped SAM:Eu^{2+}, Mn^{2+} G phosphor can be commercially used in WLEDs for backlighting systems. The color gamut of the narrow-band G-emitting SAM:0.4Eu^{2+},0.6Mn^{2+}- and R-emitting KSF:Mn^{4+}-based white-by-blue (114%) is wider than that of the sharp γ-AlON:Mn^{2+}, Mg^{2+} G- and the KSF:Mn^{4+} R phosphor-based tricolor white LED (102%), which is one of the largest color gamut outcomes reproduced by color-filtered inorganic phosphors of white DC-WLEDs in reported publications. As shown in Figure 8e, the color gamut of the LCD backlight display with the SAM:0.4Eu^{2+}, 0.6Mn^{2+} G phosphor and the KSF:Mn^{4+} R phosphor can easily cover the NTSC triangles in the 1931 CIE color space. It is necessary to increase the PLE intensity and shift the right-hand side of the PLE spectrum of the SAM:0.4Eu^{2+}, 0.6Mn^{2+} phosphor further toward a longer wavelength if this material is to be used as a narrow-band G phosphor excitable by a commercialized B LED.
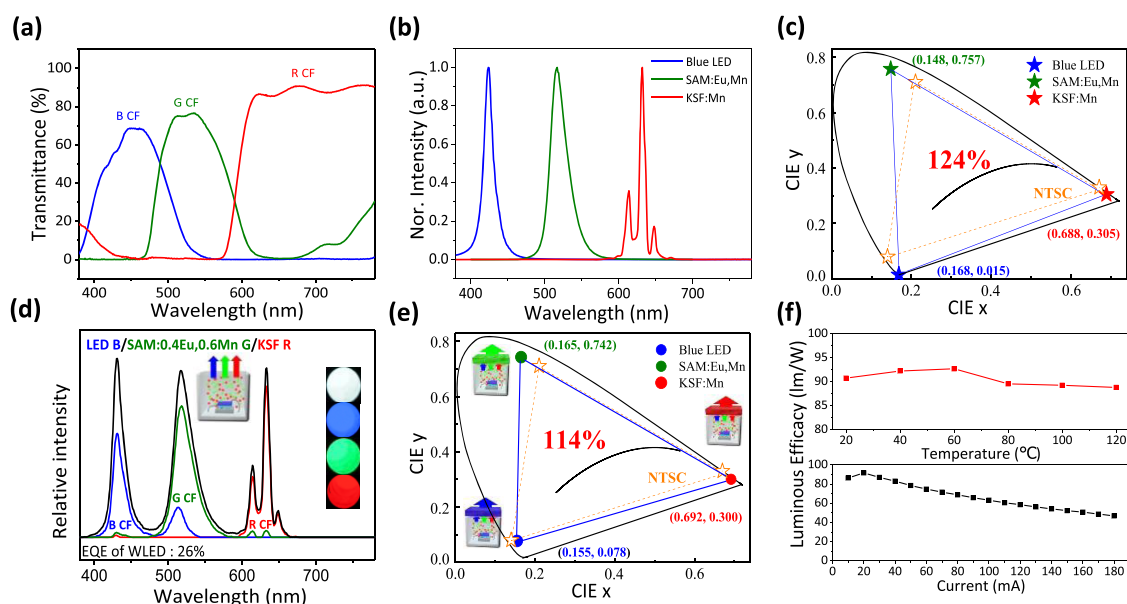
Figure 8. (a) Transmittance spectra of the blue, green, and red filters. (b) EL spectra and (c) CIE color coordinates of the B LED, SAM:0.4Eu,0.6Mn G phosphor, and the KSF:Mn R phosphor excited by a blue LED. (d) Emission spectrum of the measured RGB spectra from the filtered WLEDs excited by a blue LED. Inset: photographs of white light, filtered blue, green, and red light from a tricolor WLED incorporating the SAM:0.4Eu,0.6Mn G and KSF:Mn R phosphors. (e) CIE color coordinates of filtered RGB tricolor phosphors (11 806 K) and (f) LE value variations of a DC-WLED incorporated with SAM:0.4Eu,0.6Mn G and KSF:Mn R phosphors as a function of applied current (mA) and operating temperature (°C).

CONCLUSIONS

By optimizing up to a high wavelength of 428 nm d intensity of the PLE spectrum and the red shift of the PLE band-edge from violet to deep blue color for Eu- and Mn-co-doped G phosphors having β-alumina structure, an efficient SAM:0.4Eu^{2+}, 0.6Mn^{2+} G phosphor was developed. The newly designed phosphor is a good candidate narrow-band B-excitable G-emitting phosphor. The relative PLQYs of the SAM:0.4Eu^{2+}, 0.6Mn^{2+} phosphor were calculated and found to be 1.43, 0.97, 0.98, and 0.26, comparable to those of the YAG:Ce^{3+} phosphor (PLQY = ~0.95 at 400−450 nm) at 418, 424, 432, and 447 nm excitation wavelengths, respectively. This good PLQY value at deep blue excitation was obtained by efficient energy transfer between Eu^{2+} and Mn^{2+} ions of the SAM:0.4Eu^{2+}, 0.6Mn^{2+} G phosphor. As noted above, the high concentrations of Eu^{2+} and Mn^{2+} ions in the lattice can increase the energy transfer between Eu^{2+} ions in the conduction block and Mn^{2+} ions in the spinel block.

The color gamut areas of the unfiltered GR phosphors and the 432 nm B LED and filtered RGB triangle of tricolor DC-WLEDs incorporating SAM:0.4Eu^{2+}, 0.6Mn^{2+} G and KSF:Mn^{4+} R reached 124 and 114%, respectively, relative to the NTSC standard system in the 1931 CIE color space. The peak positions and FWHMs of the SAM:0.4Eu^{2+}, 0.6Mn^{2+} peak of white colors in the DC-WLED packages also remain unchanged relative to those of the PL emissions of the newly developed SAM:0.4Eu^{2+}, 0.6Mn^{2+} G phosphors. The measured LE of the white of tricolor white LEDs is ~92 lm/W at 20 mA. The resulting color gamut of the filtered, narrow-band SAM:0.4Eu^{2+}, 0.6Mn^{2+} G and KSF:Mn^{4+} R-based white-by-blue LED (~114%) is superior to the color gamut of the reported γ-AlON:Mn^{2+}, Mg^{2+} G and KSF:Mn^{4+} R phosphor-based tricolor WLED (~102%) and superior to that of the commercialized InP/ZnS QD-based QDEF (~100%) backlight system for LCDs. Otherwise, the resulting color gamut is slightly inferior to the widest color gamut of the reported SMAO:Mn^{2+} G- and KSF:Mn^{4+} R phosphor-based tricolor WLEDs (127%).

The increased intensity and red shift of PLE excitation, along with the improved QYs of the SAM:Eu^{2+}, Mn^{2+} phosphor represent an alternative opportunity to reuse inorganic narrow-band GR phosphors for on-chip LCD backlights with high color gamut and good flexibility.

EXPERIMENTAL SECTION

Materials and Chemicals. Strontium carbonate (SrCO$_3$, 99%, Sigma-Aldrich), europium(III) oxide (Eu$_2$O$_3$, 99.9%, Sigma-Aldrich), magnesium oxide (MgO, 99%, Sigma-Aldrich), and manganese(II) carbonate (MnCO$_3$, 99.9%, Sigma-Aldrich) were used without further purification as reactants for the solid-state reactions. Magnesium fluoride (MgF$_2$, technical grade, Sigma-Aldrich) was used as a flux material.

Synthesis of Narrow-Band SrMgAl$_{10}$O$_{17}$:Eu^{2+}, Mn^{2+} Green Phosphor. To synthesize SrMgAl$_{10}$O$_{17}$: Eu^{2+}, Mn^{2+} G phosphor, SrCO$_3$, Eu$_2$O$_3$, MgO, MnCO$_3$, and 4 wt % MgF$_2$ as flux were added, mixed using a mortar and pestle and put in an alumina crucible. The well-mixed mixture was calcined at 1500 °C for 4 h in an atmosphere of H$_2$ (5%) + N$_2$ (95%). The resulting sintered phosphor was then removed in a furnace, ground, washed, and sieved before optical and crystallographic evaluation and application to the LED.

Characterization of Phosphors. The PLE and PL of all powder phosphors were measured using a spectrophotometer (Darsa, PSI Trading Co., Korea) with a Xe lamp, and absolute photoluminescent quantum yield (PLQY) was measured using a TCSPC spectrophotofluorometer (Fluorolog 3, HORIBA, Japan). The crystal structures of the SrMgAl$_{10}$O$_{17}$:Eu^{2+}, Mn^{2+} G phosphors were investigated by means of X-ray diffraction with Cu Kα_1 radiation (D-max 2500, JEOL). The phases of the obtained phosphors were analyzed based on a standard phase with JCPDS card no. 00-026-0879 (Standard SAM). Structural analysis of the synthesized compounds was conducted through Rietveld refinement of the SAM series using synchrotron diffraction data at the high-resolution powder diffraction

(HRPD) beamline (9B) of the Pohang Accelerator Laboratory (PAL). During the measurements, $\theta/2\theta$ with a fixed time of 1 s and step size of 0.01° for 2θ = 0−130° and beamline with a wavelength of 1.52250 Å were used. Refinement was performed using the General Structure Analysis System (GSAS) package with a split pseudo-Voigt function defining the profile shape; a polynomial of the first degree was used to define the background.[47] The background coefficients, zero point, half-width, pseudo-Voigt, asymmetry parameters of peak shape, scale factor, and unit cell parameters were refined until convergence was obtained. Using a field emission scanning electron microscope (FE-SEM, JEM- 7610F, JEOL, Japan), the morphology of the phosphors was measured after grinding, washing, and sieving.

Fabrication of Single-Package DC-WLED. SAM:0.4Eu²⁺, 0.6Mn²⁺ G phosphors and KSF:Mn⁴⁺ R phosphors were dispersed in a silicon binder (OE-6636A and OE-6636B, Dow Corning, Korea) to form phosphor pastes. To compare the optical characteristics, a DC-WLED was fabricated using an on-chip white-by-blue configuration by mixing phosphors at a G-to-R ratio of 2:1 at 60 wt % with a silicon binder. To fabricate single-package WLEDs, the paste was initially used to fill a BLED (λ_{max} = 432 nm, Seoul Semiconductor, Inc., Korea). Subsequently, the packages were dried and hardened at 150 °C for 1 h.

ASSOCIATED CONTENT

ⓢ Supporting Information

The Supporting Information is available free of charge at https://pubs.acs.org/doi/10.1021/acsomega.0c01798.

Relative PLQYs and other optical properties of three different G phosphors (Table S1); Rietveld refinement and crystal parameter data (Table S2); structural parameters (Table S3); Rietveld refinement results of the synchrotron diffraction profile (Figure S1); evolution of lattice parameters as a function of x (Figure S2); and evolution of lattice parameters as a function of y (Figure S3) (PDF)

AUTHOR INFORMATION

Corresponding Authors

Won Bin Im − *Division of Materials Science and Engineering, Hanyang University, Seoul 04763, Republic of Korea;* ⓘ orcid.org/0000-0003-2473-4714; Email: imwonbin@hanyang.ac.kr

Young Rag Do − *Department of Chemistry, Kookmin University, Seoul 02703, Republic of Korea;* ⓘ orcid.org/0000-0002-0580-4628; Email: yrdo@kookmin.ac.kr

Authors

Heejoon Kang − *Department of Chemistry, Kookmin University, Seoul 02703, Republic of Korea*

Keyong Nam Lee − *Department of Chemistry, Kookmin University, Seoul 02703, Republic of Korea*

Sanjith Unithrattil − *School of Materials Science and Engineering, Gwangju Institute of Science and Technology, Gwangju 61005, Republic of Korea;* ⓘ orcid.org/0000-0001-9072-7163

Ha Jun Kim − *Division of Materials Science and Engineering, Hanyang University, Seoul 04763, Republic of Korea*

Ji Hye Oh − *Department of Chemistry, Kookmin University, Seoul 02703, Republic of Korea*

Jae Soo Yoo − *Department of Chemical Engineering, Chung-Ang University, Seoul 06973, Republic of Korea*

REFERENCES

(1) Jang, E.; Jun, S.; Jang, H.; Lim, J.; Kim, B.; Kim, Y. White-light-emitting diodes with quantum dot color converters for display backlights. *Adv. Mater.* **2010**, *22*, 3076−3080.

(2) Coe-Sullivan, S.; Liu, W.; Allen, P.; Steckel, J. S. Quantum dots for LED downconversion in display applications. *ECS J. Solid State Sci. Technol.* **2013**, *2*, R3026−R3030.

(3) Chen, J.; Hardev, V.; Hartlove, J.; Hofler, J.; Lee, E. In 66.1: Distinguised Paper: A High-Efficiency Wide-Color-Gamut Solid-State Backlight System for LCDs Using Quantum Dot Enhancement Film. In *SID Symposium Digest of Technical Papers*; Wiley Online Library, 2012; Vol. *43*, pp 895−896.

(4) Luo, Z.; Xu, D.; Wu, S.-T. Emerging quantum-dots-enhanced LCDs. *J. Disp. Technol.* **2014**, *10*, 526−539.

(5) Luo, Z.; Chen, Y.; Wu, S.-T. Wide color gamut LCD with a quantum dot backlight. *Opt. Express* **2013**, *21*, 26269−26284.

(6) Yoshimura, K.; Fukunaga, H.; Izumi, M.; Masuda, M.; Uemura, T.; Takahashi, K.; Xie, R. J.; Hirosaki, N. White LEDs using the sharp β-sialon: Eu phosphor and Mn-doped red phosphor for wide-color gamut display applications. *J. Soc. Inf. Disp.* **2016**, *24*, 449−453.

(7) Todescato, F.; Fortunati, I.; Minotto, A.; Signorini, R.; Jasieniak, J. J.; Bozio, R. Engineering of semiconductor nanocrystals for light emitting applications. *Materials* **2016**, *9*, No. 672.

(8) Boles, M. A.; Ling, D.; Hyeon, T.; Talapin, D. V. The surface science of nanocrystals. *Nat. Mater.* **2016**, *15*, 141.

(9) Byun, H.-J.; Song, W.-S.; Yang, H. Facile consecutive solvothermal growth of highly fluorescent InP/ZnS core/shell quantum dots using a safer phosphorus source. *Nanotechnology* **2011**, *22*, No. 235605.

(10) Yang, S. J.; Oh, J. H.; Kim, S.; Yang, H.; Do, Y. R. Realization of InP/ZnS quantum dots for green, amber and red down-converted LEDs and their color-tunable, four-package white LEDs. *J. Mater. Chem. C* **2015**, *3*, 3582−3591.

(11) Lee, S.-H.; Lee, K.-H.; Jo, J.-H.; Park, B.; Kwon, Y.; Jang, H. S.; Yang, H. Remote-type, high-color gamut white light-emitting diode based on InP quantum dot color converters. *Opt. Mater. Express* **2014**, *4*, 1297−1302.

(12) Ramasamy, P.; Kim, B.; Lee, M.-S.; Lee, J.-S. Beneficial effects of water in the colloidal synthesis of InP/ZnS core−shell quantum dots for optoelectronic applications. *Nanoscale* **2016**, *8*, 17159−17168.

(13) Protesescu, L.; Yakunin, S.; Bodnarchuk, M. I.; Krieg, F.; Caputo, R.; Hendon, C. H.; Yang, R. X.; Walsh, A.; Kovalenko, M. V. Nanocrystals of cesium lead halide perovskites ($CsPbX_3$, X= Cl, Br, and I): novel optoelectronic materials showing bright emission with wide color gamut. *Nano Lett.* **2015**, *15*, 3692−3696.

(14) Nedelcu, G.; Protesescu, L.; Yakunin, S.; Bodnarchuk, M. I.; Grotevent, M. J.; Kovalenko, M. V. Fast anion-exchange in highly luminescent nanocrystals of cesium lead halide perovskites ($CsPbX_3$, X= Cl, Br, I). *Nano Lett.* **2015**, *15*, 5635−5640.

(15) Yoon, H. C.; Kang, H.; Lee, S.; Oh, J. H.; Yang, H.; Do, Y. R. Study of perovskite QD down-converted LEDs and six-color white LEDs for future displays with excellent color performance. *ACS Appl. Mater. Interfaces* **2016**, *8*, 18189−18200.

(16) Zhang, F.; Zhong, H.; Chen, C.; Wu, X.-g.; Hu, X.; Huang, H.; Han, J.; Zou, B.; Dong, Y. Brightly luminescent and color-tunable colloidal CH3NH3PbX3 (X= Br, I, Cl) quantum dots: potential alternatives for display technology. *ACS Nano* **2015**, *9*, 4533−4542.

(17) Adachi, S.; Takahashi, T. Direct synthesis of K2SiF6: Mn4+ red phosphor from crushed quartz schist by wet chemical etching. *Electrochem. Solid-State Lett.* **2009**, *12*, J20−J23.

(18) Oh, J. H.; Kang, H.; Eo, Y. J.; Park, H. K.; Do, Y. R. Synthesis of narrow-band red-emitting K2SiF6:Mn4+ phosphors for a deep red monochromatic LED and ultrahigh color quality warm-white LEDs. *J. Mater. Chem. C* **2015**, *3*, 607−615.

(19) Moon, J. W.; Min, B. G.; Kim, J. S.; Jang, M. S.; Ok, K. M.; Han, K.-Y.; Yoo, J. S. Optical characteristics and longevity of the line-emitting K2SiF6:Mn⁴⁺ phosphor for LED application. *Opt. Mater. Express* **2016**, *6*, 782−792.

(20) Steckel, J. S.; Ho, J.; Hamilton, C.; Xi, J.; Breen, C.; Liu, W.; Allen, P.; Coe-Sullivan, S. Quantum dots: The ultimate down-conversion material for LCD displays. *J. Soc. Inf. Disp.* **2015**, *23*, 294−305.

(21) Xie, R.-J.; Hirosaki, N.; Takeda, T. Wide color gamut backlight for liquid crystal displays using three-band phosphor-converted white light-emitting diodes. *Appl. Phys. Express* **2009**, *2*, No. 022401.

(22) Fukuda, Y.; Matsuda, N.; Okada, A.; Mitsuishi, I. White light-emitting diodes for wide-color-gamut backlight using green-emitting Sr-sialon phosphor. *Jpn. J. Appl. Phys.* **2012**, *51*, No. 122101.

(23) Oh, J. H.; Kang, H.; Ko, M.; Do, Y. R. Analysis of wide color gamut of green/red bilayered freestanding phosphor film-capped white LEDs for LCD backlight. *Opt. Express* **2015**, *23*, A791−A804.

(24) Wang, L.; Wang, X.; Kohsei, T.; Yoshimura, K.-i.; Izumi, M.; Hirosaki, N.; Xie, R.-J. Highly efficient narrow-band green and red phosphors enabling wide color-gamut LED backlight for more brilliant displays. *Opt. Express* **2015**, *23*, 28707−28717.

(25) Takahashi, K.; Xie, R.-J.; Hirosaki, N. Toward higher color purity and narrower emission band β-sialon: Eu²⁺ by reducing the oxygen concentration. *Electrochem. Solid-State Lett.* **2011**, *14*, E38−E40.

(26) Yasushi, I.; Tomomitsu, H.; Tsuneo, K.; Hiroshi, N.; Hirofumi, K. A phosphor sheet and a backlight system providing wider color gamut for LCDs. *J. Soc. Inf. Disp.* **2014**, *22*, 419−428.

(27) Takeda, T.; Hirosaki, N.; Funahshi, S.; Xie, R.-J. Narrow-band green-emitting phosphor Ba₂LiSi₇AlN₁₂: Eu²⁺ with high thermal stability discovered by a single particle diagnosis approach. *Chem. Mater.* **2015**, *27*, 5892−5898.

(28) Strobel, P.; Schmiechen, S.; Siegert, M.; Tücks, A.; Schmidt, P. J.; Schnick, W. Narrow-band green emitting nitridolithoalumosilicate Ba[Li₂(Al₂Si₂)N₆]: Eu²⁺ with framework topology whj for LED/LCD-backlighting applications. *Chem. Mater.* **2015**, *27*, 6109−6115.

(29) Hirosaki, N.; Xie, R.-J.; Kimoto, K.; Sekiguchi, T.; Yamamoto, Y.; Suehiro, T.; Mitomo, M. Characterization and properties of green-emitting β-SiAlON: Eu²⁺ powder phosphors for white light-emitting diodes. *Appl. Phys. Lett.* **2005**, *86*, No. 211905.

(30) Zhang, J.; Zhou, M.; Liu, B.; Wang, Y. The Thermal Stability and Photoluminescence Degradation of Mn²⁺ in Fluorescent Lamp used BaMgAl10O17: Eu²⁺, Mn2+ Phosphor. *Int. J. Appl. Ceram. Technol.* **2013**, *10*, 638−642.

(31) Okamoto, S.; Yamamoto, H. Photoluminescence Properties of BaMgAl10O17 Doped with High Concentration of Mn²⁺ for Blue-LED-Based Solid-State Lighting. *J. Electrochem. Soc.* **2011**, *158*, J363−J367.

(32) Ke, W.-C.; Lin, C. C.; Liu, R.-S.; Kuo, M.-C. Energy transfer and significant improvement moist stability of BaMgAl10O17:Eu²⁺, Mn²⁺ as a phosphor for white light-emitting diodes. *J. Electrochem. Soc.* **2010**, *157*, J307−J309.

(33) Endou, A.; Hiroaki, O.; Hiromi, K.; Itaru, Y.; Kazumi, S.; Kenji, I.; Ryo, S.; Michihisa, K.; Hideyuki, T.; Nozomu, H.; Hiromitsu, T.; Carlos, A. D. C.; Momoji, K.; Hiroshi, K.; Akira, M. A. Theoretical Study of Initial Deposition Processes of Mg on MgO: A Novel Quantum Chemical Molecular Dynamics Approach. *Jpn. J. Appl. Phys.* **2009**, *48*, No. 04C126.

(34) Dawson, B.; Ferguson, M.; Marking, G.; Diaz, A. L. Mechanisms of VUV damage in BaMgAl10O17: Eu²⁺. *Chem. Mater.* **2004**, *16*, 5311−5317.

(35) Zhang, A.; Akashi, T.; Zhang, B. P.; Goto, T. Electrical conductivity of partially ion exchanged Sr and Ba β-alumina single crystals determined by a.c. impedance spectroscopy. *Mater. Lett.* **2006**, *60*, 2834−2836.

(36) Krupa, J. C.; Queffelec, M. UV and VUV optical excitations in wide band gap materials doped with rare earth ions: 4f−5d transitions. *J. Alloys Compd.* **1997**, *250*, 287−292.

(37) Chen, Z.; Yan, Y. Morphology control and VUV photo-luminescence characteristics of BaMgAl10O17:Eu²⁺ phosphors. *Phys. B* **2007**, *392*, 1−6.

(38) Yang, W.-J.; Luo, L.; Chen, T.-M.; Wang, N.-S. Luminescence and energy transfer of Eu-and Mn-coactivated CaAl₂Si₂O₈ as a potential phosphor for white-light UVLED. *Chem. Mater.* **2005**, *17*, 3883−3888.

(39) Zhu, Y.; Liang, Y.; Liu, S.; Li, H.; Chen, J. Narrow-Band Green-Emitting Sr2MgAl22O36:Mn²⁺ Phosphors with Superior Thermal Stability and Wide Color Gamut for Backlighting Display Applications. *Adv. Opt. Mater.* **2019**, *7*, No. 1801419.

(40) Wang, B.; Lin, H.; Huang, F.; Xu, J.; Chen, H.; Lin, Z.; Wang, Y. Non-Rare-Earth BaMgAl₁₀₋₂ₓO₁₇:ₓMn⁴⁺,xMg²⁺: A Narrow-Band Red Phosphor for Use as a High-Power Warm w-LED. *Chem. Mater.* **2016**, *28*, 3515−3524.

(41) Howe, B.; Diaz, A.-L. Characterization of host-lattice emission and energy transfer in BaMgAl10O17:Eu²⁺. *J. Lumin.* **2004**, *109*, 51−59.

(42) Zhang, S.; Kokubu, M.; Fujii, H.; Uchiike, H. A study on the choromaticity shifts of blue phosphor for color plasma displays. *J. Soc. Inf. Disp.* **2002**, *10*, 25−29.

(43) Yoshimura, K.; Fukunaga, H.; Izumi, M.; Takahashi, K.; Xie, R.-J.; Hirosaki, N. Achieving superwide-color-gamut display by using narrow-band green-emitting γ-AlON:Mn,Mg phosphor. *Jpn. J. Appl. Phys.* **2017**, *56*, No. 041701.

(44) Zhao, M.; Liao, H.; Ning, L.; Zhang, Q.; Liu, Q.; Xia, Z. Next-Generation Narrow-Band Green-Emitting RbLi(Li₃SiO₄)₂:Eu²⁺ Phosphor for Backlight Display Application. *Adv. Mater.* **2018**, *30*, No. 1802489.

(45) Liao, H.; Zhao, M.; Zhou, Y.; Molokeev, M. S.; Liu, Q.; Zhang, Q.; Xia, Z. Polyhedron Transformation toward Stable Narrow-Band Green Phosphors for Wide-Color-Gamut Liquid Crystal Display. *Adv. Funct. Mater.* **2018**, *29*, No. 1901988.

(46) Shannon, R. D. Revised Effective Ionic Radii and Systematic Studies of Interatomic Distances in Halides and Chalcogenides. *Acta Crystallogr., Sect. A: Cryst. Phys., Diffr., Theor. Gen. Crystallogr.* **1976**, *A32*, 751.

(47) Allen, C. L.; Robert, B. V. D. *General Structure Analysis System (GSAS)*, LAUR 86-748; Los Alamos National Laboratory, 2004.